nature genetics

Identification of 153 new loci associated with heel bone mineral density and functional involvement of GPC6 in osteoporosis

John P Kemp[1,2,25], John A Morris[3,4,25], Carolina Medina-Gomez[5,6,25], Vincenzo Forgetta[3], Nicole M Warrington[1,7], Scott E Youlten[8,9], Jie Zheng[2], Celia L Gregson[10], Elin Grundberg[4], Katerina Trajanoska[5,6], John G Logan[11], Andrea S Pollard[11], Penny C Sparkes[11], Elena J Ghirardello[11], Rebecca Allen[11], Victoria D Leitch[11], Natalie C Butterfield[11], Davide Komla-Ebri[11], Anne-Tounsia Adoum[11], Katharine F Curry[11], Jacqueline K White[12], Fiona Kussy[12], Keelin M Greenlaw[3], Changjiang Xu[13], Nicholas C Harvey[14,15], Cyrus Cooper[14,15,16], David J Adams[12], Celia M T Greenwood[3,4,17,18], Matthew T Maurano[19], Stephen Kaptoge[20,21], Fernando Rivadeneira[5,6], Jonathan H Tobias[10], Peter I Croucher[8,9,22], Cheryl L Ackert-Bicknell[23], J H Duncan Bassett[11], Graham R Williams[11], J Brent Richards[3,4,24,26] & David M Evans[1,2,26]

Osteoporosis is a common disease diagnosed primarily by measurement of bone mineral density (BMD). We undertook a genome-wide association study (GWAS) in 142,487 individuals from the UK Biobank to identify loci associated with BMD as estimated by quantitative ultrasound of the heel. We identified 307 conditionally independent single-nucleotide polymorphisms (SNPs) that attained genome-wide significance at 203 loci, explaining approximately 12% of the phenotypic variance. These included 153 previously unreported loci, and several rare variants with large effect sizes. To investigate the underlying mechanisms, we undertook (1) bioinformatic, functional genomic annotation and human osteoblast expression studies; (2) gene-function prediction; (3) skeletal phenotyping of 120 knockout mice with deletions of genes adjacent to lead independent SNPs; and (4) analysis of gene expression in mouse osteoblasts, osteocytes and osteoclasts. The results implicate *GPC6* as a novel determinant of BMD, and also identify abnormal skeletal phenotypes in knockout mice associated with a further 100 prioritized genes.

Osteoporosis is a common age-related disorder characterized by low bone mass and deterioration in bone microarchitecture, leading to increased skeletal fragility and fracture risk. Low BMD is a strong risk factor for osteoporosis, as well as a key indicator for its diagnosis and treatment[1]. BMD is highly heritable[2], and GWASs have identified common variants at 73 loci associated with the trait, including many that are significantly associated with fracture risk[3,4]. Recently, deep imputation based on whole-genome sequencing has also identified low-frequency variants of large effect associated with BMD and fracture risk[4]. Despite these advances, common and rare variants explain only 5.8% of the total phenotypic variance in BMD[3,4].

In most previous genetic studies of BMD, the data analyzed were derived from dual-energy X-ray absorptiometry (DXA). However, DXA is expensive, and consequently the largest GWAS so far of DXA-derived BMD included only 32,965 individuals[4], which compromised the researchers' ability to detect risk loci. An alternative method of

[1]University of Queensland Diamantina Institute, Translational Research Institute, Brisbane, Queensland, Australia. [2]MRC Integrative Epidemiology Unit, University of Bristol, Bristol, UK. [3]Centre for Clinical Epidemiology, Lady Davis Institute, Jewish General Hospital, McGill University, Montréal, Québec, Canada. [4]Department of Human Genetics, McGill University, Montréal, Québec, Canada. [5]Department of Internal Medicine, Erasmus Medical Center, Rotterdam, the Netherlands. [6]Department of Epidemiology, Erasmus Medical Center, Rotterdam, the Netherlands. [7]Division of Obstetrics and Gynaecology, The University of Western Australia, Perth, Western Australia, Australia. [8]Garvan Institute of Medical Research, Sydney, New South Wales, Australia. [9]St. Vincent's Clinical School, University of New South Wales, Sydney, New South Wales, Australia. [10]Musculoskeletal Research Unit, Department of Translational Health Sciences, University of Bristol, Bristol, UK. [11]Molecular Endocrinology Laboratory, Department of Medicine, Imperial College London, London, UK. [12]Wellcome Trust Sanger Institute, Wellcome Trust Genome Campus, Hinxton, Cambridgeshire, UK. [13]Donnelly Center for Cellular and Biomedical Research, University of Toronto, Toronto, Ontario, Canada. [14]MRC Lifecourse Epidemiology Unit, University of Southampton, Southampton, UK. [15]NIHR Southampton Biomedical Research Centre, University of Southampton and University Hospital Southampton NHS Foundation Trust, Southampton, UK. [16]NIHR Oxford Biomedical Research Centre, University of Oxford, Oxford, UK. [17]Gerald Bronfman Department of Oncology, McGill University, Montréal, Québec, Canada. [18]Department of Epidemiology, Biostatistics & Occupational Health, McGill University, Montréal, Québec, Canada. [19]Department of Pathology and Institute for Systems Genetics, New York University Langone Medical Center, New York, New York, USA. [20]Department of Public Health and Primary Care, University of Cambridge, Cambridge, UK. [21]Strangeways Research Laboratory, Cambridge, UK. [22]School of Biotechnology and Biomolecular Sciences, University of New South Wales, Sydney, New South Wales, Australia. [23]Center for Musculoskeletal Research, Department of Orthopaedics, University of Rochester, Rochester, New York, USA. [24]Department of Twin Research and Genetic Epidemiology, King's College London, London, UK. [25]These authors contributed equally to this work. [26]These authors jointly supervised this work. Correspondence should be addressed to D.M.E. (d.evans1@uq.edu.au) or J.B.R. (brent.richards@mcgill.ca).

Received 31 December 2016; accepted 11 August 2017; published online 4 September 2017; doi:10.1038/ng.3949

estimating BMD that is quick, safe and relatively inexpensive, and therefore can be used in very large samples of individuals, is derived from ultrasound, typically at the heel calcaneus (referred to here as estimated BMD (eBMD)). Ultrasound-derived eBMD values are highly heritable (on the order of 50% to 80%)[5–8], independently associated with fracture risk[9,10] and moderately correlated with DXA-derived BMD at the hip and spine (r = 0.4–0.6)[11]. A previous GWAS that used heel ultrasound parameters (N = 15,514) identified variants at nine loci, including seven that had been previously associated with lumbar spine/hip BMD[12].

Because genetic loci associated with BMD are strongly enriched for the targets of clinically relevant osteoporosis therapies[13,14], the identification of new genetic loci and the biological pathways they implicate may help scientists identify drug targets for the prevention and treatment of fragility fracture. To identify novel genetic determinants of BMD, we investigated genome-wide association in the UK Biobank Study, which has measured eBMD and genome-wide genotypes in 142,487 individuals. We subsequently used three systematic and complementary approaches to prioritize genes for functional validation (**Supplementary Fig. 1**).

RESULTS

Genome-wide association study of estimated BMD

Quantitative ultrasound of the heel was used to obtain a non-invasive estimate of BMD that predicts fracture[9,10]. After stringent quality control of both eBMD measurements and genome-wide genotypes (Online Methods, **Supplementary Fig. 2**), data were available from 142,487 individuals (53% women) (**Supplementary Table 1**). We tested the additive effect of 17,166,351 SNPs with minor allele frequency (MAF) > 0.1% and imputation quality score > 0.4 on eBMD, controlling for age, sex and genotyping array. In total, 307 conditionally independent SNPs at 203 loci surpassed our revised genome-wide significance threshold ($P \leq 6.6 \times 10^{-9}$, which accounts for the large number of independent SNPs deeply imputed in the UK Biobank (Online Methods)) and jointly explained ~12% of the variance in eBMD (**Supplementary Fig. 3**, **Supplementary Table 2**). Together the 307 SNPs explained about one-third of the eBMD SNP heritability estimated by BOLT-REML (h^2_{SNP} = 0.36). Although there was substantial inflation of the test statistics relative to the null (λ_{GC} = 1.37), linkage disequilibrium (LD) score regression[15] indicated that the majority of inflation was due to polygenicity rather than population stratification (LD score regression intercept = 1.05). Of the 203 loci identified, 153 (75%) regions had not been implicated in previous GWASs of BMD[3,4,16–22] (**Supplementary Table 2**, **Supplementary Fig. 3**). We found it interesting that the list of novel associations included multiple variants (e.g., SNPs at *TBX1*, *ZNRF3*) for which there was extremely strong evidence of association with heel eBMD ($P < 10^{-30}$) but little evidence of association ($P > 0.05$ for any trait) in a previous GEFOS-seq GWAS of DXA-derived BMD[4] (**Supplementary Table 3**).

Our study also replicated SNPs in 55 out of 73 regions (>75%) that had been reported as genome-wide significant in previous GWASs of BMD at other body sites ($P < 0.05$ and consistent direction of effect), and we replicated all loci with genome-wide significance identified in a previous GWAS of ultrasound-derived heel eBMD[12] (**Supplementary Table 4**). Our list of known BMD-associated SNPs is deliberately broad and comprehensive with respect to previous GWASs. This comprehensive inclusion policy, however, called for the

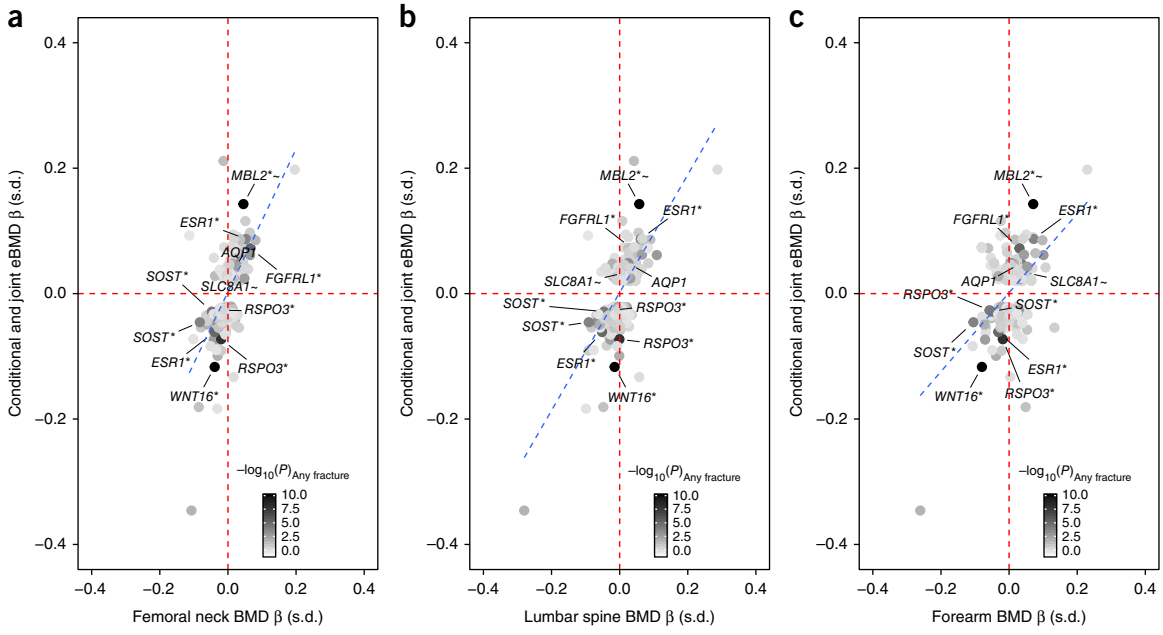

Figure 1 eBMD effect size compared with the effect size from a previous GEFOS meta-analysis of DXA-derived BMD for eBMD-associated SNPs. (**a**–**c**) Effect size for heel eBMD (*y*-axis) from the current UK Biobank study plotted against effect size from the previous GEFOS-seq study[4] for BMD at the (**a**) femoral neck, (**b**) lumbar spine and (**c**) forearm (*x*-axis). Only conditionally independent variants that reached genome-wide significance ($P < 6.6 \times 10^{-9}$) for eBMD in the UK Biobank study are plotted. The $-\log_{10}P$ value for the (any) fracture analysis of UK Biobank subjects is indicated by the shading of the data points (black indicates robust evidence of association with fracture, and white indicates poor evidence of association). SNPs that reached Bonferroni-corrected significance for fracture ($P < 1.6 \times 10^{-4}$) are labeled. The blue dashed lines show the strong correlation between estimated effect sizes at the heel and at other sites of the body. SNPs at *SLC8A1* and *AQP1* were significantly related with fracture after correction for multiple testing ($P < 1.6 \times 10^{-4}$) and have not previously been reported as associated with BMD or fracture, although they both reached nominal significance ($P < 0.05$) in the previous GEFOS-seq analysis.*Multiple conditionally independent variants present at the locus. ~The closest gene to the locus (i.e., DEPICT did not detect any region within 1 Mb of the reported SNP).

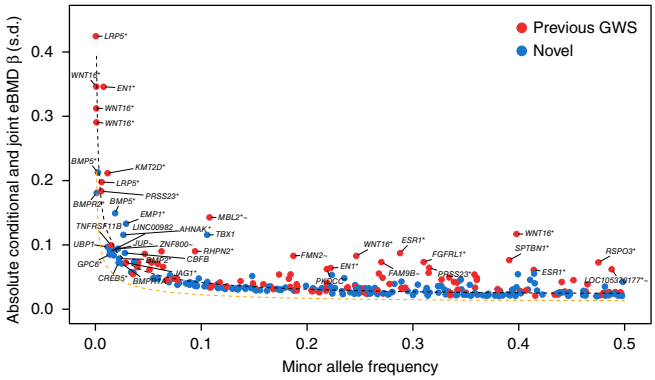

Figure 2 The relationship between absolute conditional and joint-analysis effect size (*y*-axis) and minor allele frequency (*x*-axis) for 307 conditionally independent SNPs. Red circles represent SNPs at previously reported BMD loci. Blue circles represent SNPs at novel loci. The black dashed curve shows the effect size required for 80% power to detect association at a given minor allele frequency at genome-wide significance ($\alpha = 6.6 \times 10^{-9}$) in the present study. The orange dashed curve shows the effect size required for 80% power to detect association at a given minor allele frequency at genome-wide significance ($\alpha = 6.6 \times 10^{-9}$) assuming $N = 483{,}230$ individuals in the full UK Biobank study. GWS, genome-wide significant. *Multiple conditionally independent variants present at the locus. ~The closest gene to the locus (i.e., DEPICT did not detect any region within 1 Mb of the reported SNP).

incorporation of results from some smaller GWASs that may include false positives. When we restricted our attention to the 64 SNPs reported in the large Genetic Factors for Osteoporosis Consortium (GEFOS) meta-analysis by Estrada *et al.*[3] (which are unlikely to represent type 1 errors), we replicated 54 of the 64 (84%) SNPs. Possible reasons for nonreplicated loci include site specificity, differences in phenotype (ultrasound-derived versus DXA-derived BMD), differences in ancestral population between studies, and type 1 error in the previous, smaller study.

Notably, across six loci (*RSPO3*, *LINC00326*, *CPED1*, *MPP7*, *KCNMA1* and *TMEM263*), there were SNPs with different directions of effect in the current eBMD study compared with those in previous BMD studies. The SNPs at *CPED1* also showed an association with fracture in the UK Biobank data (discussed below), but in the direction predicted by eBMD rather than the direction predicted by BMD in previous studies (i.e., alleles that predispose subjects to low eBMD are associated with increased risk of fracture). Although these opposite directions of association are difficult to explain, differences in the phenotypes measured by DXA and ultrasound technologies are likely to be responsible. For example, whereas heel ultrasound measures primarily trabecular bone, DXA-based BMD measurements reflect a combination of trabecular and cortical bone. In addition, ultrasound-based measurements are independent of bone size, whereas areal BMD as measured by DXA is not fully size-corrected. In fact, of the six loci that showed opposite associations between DXA BMD and eBMD, three also showed strong associations with height in data from the Genetic Investigation of Anthropometric Traits (GIANT) consortium in the same direction as the DXA BMD data[23], which suggests that these three associations may partly have reflected size effects (although it must be noted that several other concordant eBMD and DXA BMD loci also showed associations with height). Whereas bone size and bone mass generally show a strong positive correlation, genetic influences that lead to greater bone size might be inversely related to trabecular bone density at certain sites, owing to reduced mechanical strain as a consequence of a larger and thus stronger skeleton. However, despite these few discrepancies, overall there was a strong positive correlation between estimated effect size for the genome-wide-significant heel eBMD SNPs in the present UK Biobank Study and estimated effect sizes for DXA-derived BMD at other skeletal sites in our previous GEFOS-seq study (femoral neck, Pearson's $r = 0.64$ (0.57–0.71); lumbar spine, $r = 0.69$ (0.62–0.75); forearm, $r = 0.49$ (0.39–0.58)) (**Fig. 1**)[4]. Adjusting for weight had little effect on genome-wide significance, save for partially attenuating the strength of the association between eBMD and known adiposity variants (**Supplementary Table 5**).

Because we had used a large sample size and genotyped and/or imputed low-frequency variants (MAF < 1%), we next assessed the relationship between allelic architecture and eBMD (**Fig. 2**). We found a strong relationship between MAF and effect size that generally followed the statistical power of our study design. The variants of largest effect (for which each allele increased eBMD by 0.44 s.d.; $P = 5 \times 10^{-11}$) were in the gene *IGHMBP2* (within 0.5 Mb of known variants in *LRP5*) and the known *EN1* and *WNT16*/*CPED1* loci. We also detected several rare (MAF < 1%) and low-frequency variants (1% < MAF < 5%)

Table 1 Genome-wide significant eBMD-associated SNPs significantly associated with risk of fracture ($P < 1.6 \times 10^{-4}$)

							Any fracture				Fall fracture				
RSID	CHR	BP	C.GENE	EA	NEA	EAF	OR	$CI_{95\%-L}$	$CI_{95\%-U}$	*P*	OR	$CI_{95\%-L}$	$CI_{95\%-U}$	*P*	Status
rs10490046	2	40630678	*SLC8A1*	A	C	0.78	0.94	0.92	0.97	6.8×10^{-6}	0.94	0.91	0.98	1.4×10^{-3}	Novel
rs112069922	4	1034997	*IDUA*	C	T	0.95	0.89	0.84	0.93	4.8×10^{-6}	0.90	0.84	0.96	2.2×10^{-3}	Known
rs9491689	6	127398595	*RSPO3*	C	A	0.72	1.05	1.03	1.08	5.0×10^{-5}	1.05	1.02	1.09	2.0×10^{-3}	Known
rs7741021	6	127468274	*RSPO3*	A	C	0.52	1.07	1.04	1.09	1.5×10^{-8}	1.07	1.04	1.10	4.8×10^{-6}	Known
rs4869744	6	151908012	*ESR1*	T	C	0.71	0.95	0.93	0.98	1.3×10^{-4}	0.95	0.92	0.98	8.0×10^{-4}	Known
rs2941741	6	152008982	*ESR1*	G	A	0.58	1.05	1.03	1.08	6.5×10^{-6}	1.07	1.04	1.11	2.4×10^{-6}	Known
rs10276670	7	30956489	*AQP1*	A	G	0.77	0.95	0.92	0.97	4.1×10^{-5}	0.94	0.91	0.97	3.5×10^{-4}	Novel
rs2536195	7	120959155	*WNT16*	A	G	0.6	1.10	1.07	1.12	2.6×10^{-15}	1.13	1.10	1.16	1.6×10^{-15}	Known
rs10668066	7	120965464	*WNT16*	G	GCACC	0.75	1.09	1.07	1.12	1.5×10^{-11}	1.13	1.09	1.17	2.5×10^{-12}	Known
rs7099953	10	54426489	*MBL2*	G	T	0.89	0.90	0.87	0.93	4.9×10^{-9}	0.89	0.84	0.93	5.0×10^{-7}	Known
rs7209826	17	41796406	*SOST*	A	G	0.62	1.05	1.03	1.07	3.6×10^{-5}	1.06	1.03	1.10	7.1×10^{-5}	Known
rs188810925	17	41798194	*SOST*	G	A	0.92	1.09	1.04	1.14	9.2×10^{-5}	1.11	1.05	1.17	3.3×10^{-4}	Known

β and s.e. values from BOLT-LMM were transformed via the following formula: (β or s.e.)/($\mu \times (1 - \mu)$), where μ is the number of cases/number of controls. Approximate odds ratios (OR) and 95% confidence intervals ($CI_{95\%}$) were calculated from the transformed β and s.e. $CI_{95\%-L}$, lower CI limit; $CI_{95\%-U}$, upper CI limit; RSID, reference SNP cluster ID; CHR, chromosome; BP, base pair position of the variant according to human reference sequence Hg19/GRCh37; C.GENE, closest gene; EA, effect allele; NEA, non-effect allele; EAF, effect allele frequency; *P*, strength of evidence against the null hypothesis of no association between variant and self-reported fracture (i.e., *P* value); any fracture, any self-reported fracture within the past 5 years ($N = 14{,}492$ cases/130,563 controls); fall fracture, self-reported fracture within the past 5 years that occurred as the result of a simple fall ($N = 8{,}540$ cases/131,333 controls).

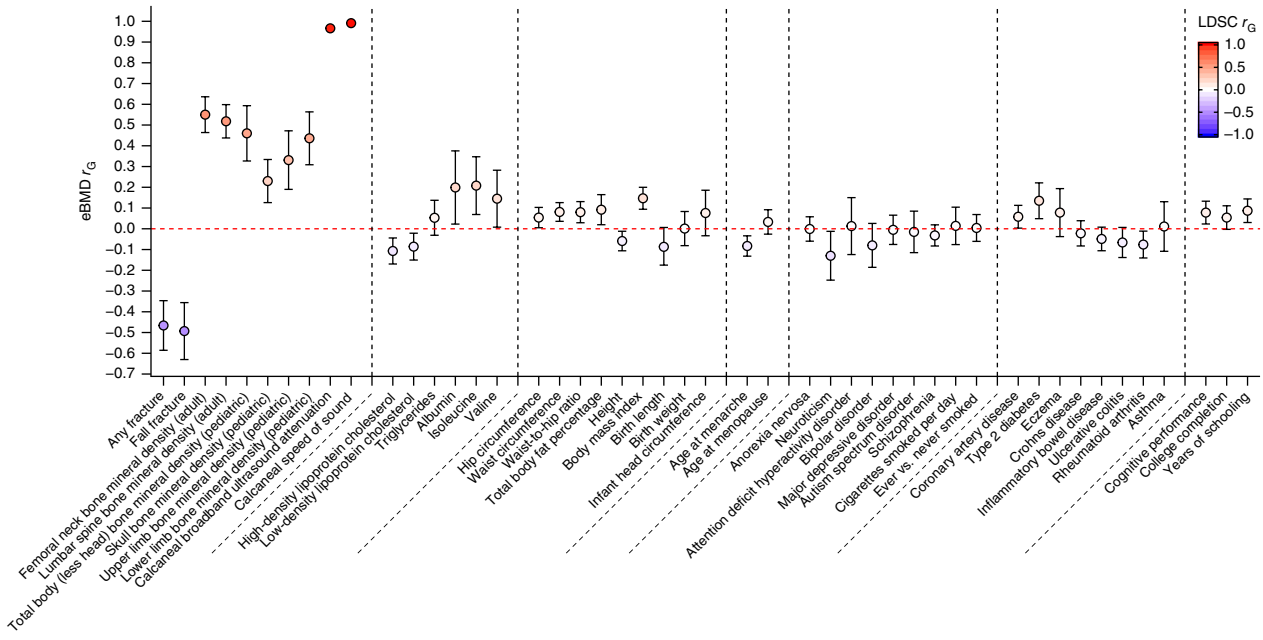

Figure 3 Genetic correlations between eBMD as measured in the UK Biobank study (*y*-axis) and other traits and diseases (*x*-axis) estimated by LD score regression implemented in LDHub. Genetic correlation (r_G) and corresponding 95% confidence intervals (error bars) between eBMD and traits were estimated via LD score regression. The genetic correlation estimates (r_G) are color-coded according to their magnitude and direction as defined in the key.

in previously unreported loci, including rare variants near the genes *BMP5* and *BMPR2*. When we compared the mean absolute effect sizes of genome-wide significant variants, we found a 6.5-fold difference in effects attributed to rare versus common variants.

Sex-specific analyses across the genome and tests of sex heterogeneity at genome-wide significant SNPs revealed a single variant, rs17307280, at *FAM9B* on the X chromosome that was significantly associated with eBMD in men only (**Supplementary Fig. 4**,

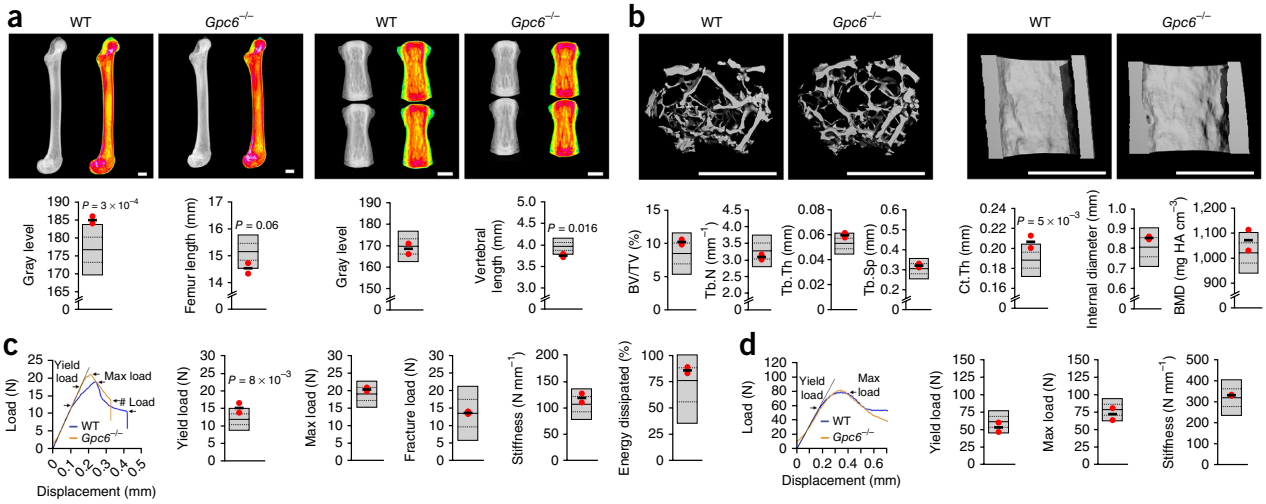

Figure 4 Increased bone mass and strength in adult *Gpc6*$^{-/-}$ mice. (**a**) X-ray microradiography images of femurs and caudal vertebrae from female wild-type (WT) and *Gpc6*$^{-/-}$ mice at postnatal day 112 (P112). In these pseudocolored grayscale images, green indicates low bone mineral content, and pink indicates high bone mineral content. The graphs at the bottom show reference ranges derived from >250 wild-type mice of identical age, sex and genetic background (C57BL/6). The plots represent the mean (solid center lines), ±1.0 s.d. (dotted lines) and ±2.0 s.d. (gray boxes). Values for parameters from individual *Gpc6*$^{-/-}$ mice are shown as red dots, and mean values as a thick black line ($n = 2$ animals). (**b**) Micro-CT images of proximal femur trabecular bone (left) and mid-diaphysis cortical bone (right) from wild-type and *Gpc6*$^{-/-}$ mice. The graphs below show trabecular bone volume/tissue volume (BV/TV), trabecular number (Tb.N), trabecular thickness (Tb.Th), trabecular spacing (Tb.Sp), cortical thickness (Ct.Th), internal cortical diameter and cortical BMD. Elements of the plots are defined as in **a**. HA, hydroxyapatite. (**c**) Representative load-displacement curves from destructive three-point bend testing of femurs from wild-type and *Gpc6*$^{-/-}$ mice, showing yield load, maximum load, fracture load and gradient of the linear elastic phase (stiffness). The graphs show yield load, maximum load, fracture load, stiffness, and energy dissipated before fracture (toughness). Elements of the plots are defined as in **a**. (**d**) Representative load-displacement curves from destructive compression testing of caudal vertebrae from wild-type and *Gpc6*$^{-/-}$ mice, showing yield load, maximum load and stiffness. Elements of the plots are defined as in **a**. *P* values were generated by permutation analysis as described in the Online Methods. Scale bars (**a**,**b**), 1 mm.

Supplementary Table 6) (heterogeneity $P = 1.4 \times 10^{-11}$), thus replicating previous results from Estrada *et al.*[3].

Effects on fracture

We tested the relationship between eBMD-associated SNPs and fracture. We identified 14,492 individuals (58% women) in UK Biobank who had reported a previous fracture, without giving special consideration to the trauma mechanism, as high-trauma fractures are predicted by low BMD and are predictive of future low-trauma fracture, thus suggesting a shared etiology[24,25]. In total, we observed that 12 eBMD SNPs were associated with fracture, after controlling for multiple testing ($P \leq 1.6 \times 10^{-4}$). The results of sensitivity analyses including only 8,540 individuals (69% women) who had reported a fracture resulting from a simple fall (i.e., from standing height) were consistent with these findings (**Table 1**). Of these 12 loci, variants at *AQP1* and *SLC8A1* had not been associated with BMD or risk of fracture previously (although both SNPs showed nominal association ($P < 0.01$) with DXA-derived BMD values from the GEFOS-seq study[4] (**Fig. 1**, **Supplementary Table 3**)). We observed an inverse relationship between the effects of genome-wide significant eBMD variants on eBMD and the odds of fracture (**Supplementary Fig. 5**).

Shared genetic factors

To test whether eBMD has a shared genetic etiology with 247 other diseases and biomedically relevant traits, we used LD score regression[26] as implemented in LDHub[27]. This method estimates the degree to which genetic risk factors are shared between two diseases or traits, although it says nothing about how this shared genetic etiology arises (i.e., whether one variable causes the other, or whether the relationship between eBMD and the other variable is mediated by an underlying variable such as body mass index (BMI), which is itself partially genetic). Genetically increased eBMD was strongly and negatively correlated with fracture (**Fig. 3**; $r_g = -0.47$; 95% CI, −0.59, −0.35). Further, measures of BMD at other skeletal sites showed moderate positive genetic correlation with eBMD (**Fig. 3**) in agreement with the concordant directions observed at the genome-wide significant loci (**Fig. 1**).

We also asked whether eBMD is genetically correlated with a range of other complex traits and diseases (**Supplementary Table 7**, **Fig. 3**). We observed weak and negative correlation with HDL cholesterol level, LDL cholesterol level, height, age at menarche and rheumatoid arthritis (**Fig. 3**). In contrast, eBMD was weakly positively genetically correlated with BMI, waist circumference, waist-to-hip ratio, coronary heart disease and type 2 diabetes. These findings support a shared genetic etiology of several common traits and diseases with eBMD, as has been shown previously for BMD, adiposity and type 2 diabetes through Mendelian randomization[28,29].

Gene prioritization

Strategy one: bioinformatic, statistical and functional genomics in humans. We used several bioinformatics and statistical genetics tools to prioritize likely candidate genes and variants. These included the Variant Effect Predictor software[30] to identify deleterious coding variation at genome-wide significant loci (**Supplementary Table 8**), the FINEMAP software to create configurations of plausible causal SNPs around each conditionally independent lead SNP (**Supplementary Table 9**), ENCODE maps of DNase I hypersensitivity sites (DHSs)[31,32] and contextual analysis of transcription factor occupancy[4] to identify SNPs that perturb transcription factor activity, and evidence of *cis*–expression quantitative trait loci (eQTLs) in human osteoblasts[33] (**Supplementary Table 10**). These results are fully described in **Supplementary Note 1**.

Strategy two: data-driven expression-prioritized integration. For the second gene-prioritization approach, we used the DEPICT computational tool[34]. We identified 273 genes as most likely to drive the eBMD association signals (false discovery rate (FDR) < 0.05). Among these 273 genes were several with an established role in bone metabolism, such as *BMP2*, *LRP5*, *EN1*, *RUNX2*, *JAG1*, *ESR1*, *COL21A1* and *SOST* (**Supplementary Table 11**).

We next tested the DEPICT-prioritized genes for enriched expression in any of 209 Medical Subject Heading (MeSH) tissue and cell-type annotations[34]. We identified 62 tissue or cell-type annotations (FDR: 5%) among the entries defined from the MeSH tissue and cell annotations (**Supplementary Table 12**, **Supplementary Fig. 6**). The strongest evidence of enriched expression of the genes mapping to eBMD loci came from chondrocytes and cartilage, although systems other than the musculoskeletal system were also overrepresented (cardiovascular system, 7/12 significant entries; membrane tissue, 6/7 significant entries; connective tissue cells, 5/7 significant entries).

We also tested the DEPICT-prioritized genes for enriched gene sets, and identified more than 1,000 significantly enriched (FDR: 5%) gene sets. Clustering in 35 'meta gene-sets' showed that most clusters were related to skeletal growth (e.g., regulation of mineralized tissue development, vertebral fusion, abnormal craniofacial development, cartilage development) or signaling pathways involved in bone biology (e.g., mesenchymal stem cell differentiation, BMP or WNT signaling). More global biological processes were also highlighted (e.g., transcription factor binding and regulation, chromatin remodeling complex, cell development) (**Supplementary Fig. 7**).

Analysis with the MAGENTA (meta-analysis gene-set enrichment of variant associations) software produced similar results implicating gene sets involved in bone mineralization and development, cadherin, the WNT and Hedgehog signaling pathways, and other pathways worthy of further investigation (oncogenic pathways, melanogenesis, etc.) (**Supplementary Table 13**).

We tested all genes prioritized by DEPICT for expression in mouse osteoblasts, osteoclasts and osteocytes. Among the 273 genes prioritized, 241 had mouse homologs (the majority that did not have a known homolog were long noncoding RNAs), with 92% expressed in osteoblasts, 66% in osteoclasts and 83% in osteocytes (**Supplementary Table 14**). In all, 95.4% of these genes were expressed in at least one of the three cell types. This represents a substantial enrichment of genes expressed in osteoblasts, osteocytes and osteoclasts ($P < 0.0001$ for each of osteoblasts, osteocytes and osteoclasts).

We then investigated whether a skeletal phenotype had been reported in the International Mouse Phenotyping Consortium (IMPC; "URLs") or Mouse Genome Informatics ("URLs") databases in knockout mice with deletion of any of the prioritized genes. We found that 189 (78%) of the 241 DEPICT-prioritized genes had mouse knockout phenotype data available, and 62 (33%) of those phenotypes included skeletal abnormalities (**Supplementary Table 14**).

Strategy three: deep phenotyping of knockout of selected genes within 1 Mb of lead SNPs. The third gene-prioritization approach identified all genes within 1 Mb of lead SNPs at associated eBMD loci. We compared these genes with genes from knockout mice generated at the Wellcome Trust Sanger Institute for the IMPC[35]. Knockout mice had been generated for 120 of the prioritized genes, and bespoke skeletal phenotyping was undertaken as part of the Origins of Bone

and Cartilage Disease Program[36]. Specifically, we carried out both structural and functional analysis of skeletal samples, using digital X-ray microradiography, micro-CT and biomechanical testing. We compared our results with normal reference data from >250 control mice with an identical C57BL/6 genetic background. We found that 43 (36%) of these 120 prioritized genes were associated with significantly abnormal bone structure, representing twofold enrichment compared with the results of a previous analysis of 100 unselected knockout mice[36] ($\chi^2 = 8.359$, $P = 0.0038$) (**Supplementary Table 15**).

GPC6 findings

Using these parallel strategies, we identified 100 genes that, when disrupted, were associated with an abnormal skeletal phenotype in mutant mice (**Supplementary Tables 14** and **15**). However, all three gene-prioritization strategies identified *GPC6*, so we selected this gene for further study (**Supplementary Table 16**).

GPC6 encodes a member of the glycosylphosphatidylinositol-anchored, membrane-bound heparan sulfate proteoglycan protein family. Loss-of-function mutations in *GPC6* result in omodysplasia 1 (OMIM 258315), a rare autosomal recessive skeletal dysplasia characterized by short-limbed dwarfism with craniofacial dysmorphism. This indicates a role for *GPC6* in skeletal biology[37], although the gene has not previously been implicated in osteoporosis.

Our bioinformatics pipeline provided evidence for a functional association at the *GPC6* locus. A single SNP in *GPC6*, rs1933784, in high linkage disequilibrium with the conditionally independent lead SNP rs147720516 at this locus ($r^2 > 0.9$), was a plausible causal and functional variant. We observed that rs1933784 was a low-frequency SNP (MAF = 0.05) that was significantly associated with eBMD ($P = 2.3 \times 10^{-10}$), with high causal probability ($\log_{10}$ Bayes factor = 2.4), and that it was present within DHSs in several cell types (**Supplementary Table 16**). The rs1933784 variant also showed some evidence of association with *GPC6* expression in osteoblasts ($P = 4.7 \times 10^{-3}$) (**Supplementary Table 16**).

DEPICT identified *GPC6* as the gene most likely to be responsible for the association at this locus. *Gpc6* is expressed in osteoblasts and osteocytes in mice (**Supplementary Table 14**). In osteocytes, *Gpc6* had a similar level of enrichment (1.76 log fold-enrichment) as genes known to have key involvement with the skeleton, such as *Lrp5* (1.95 log fold-enrichment) (**Supplementary Fig. 8**), encoding an important receptor that influences bone mass through canonical Wnt signaling, and *Runx2* (1.73 log fold-enrichment), encoding a key transcription factor in osteoblast differentiation.

We analyzed adult female *Gpc6*$^{-/-}$ mice and compared the results with data for >250 wild-type control mice of identical C57BL/6 background. Consistent with the phenotype of omodysplasia 1, *Gpc6*$^{-/-}$mice had femurs and vertebrae that were shorter than those of wild-type mice (−1.95 and −2.17 s.d., permuted $P = 0.06$ and 0.016, respectively). *Gpc6*$^{-/-}$ mice also had increased femoral bone mineral content (+2.4 s.d., permuted $P = 3 \times 10^{-4}$) and increased cortical thickness (+2.3 s.d., permuted $P = 5 \times 10^{-3}$) compared with wild-type mice. The biomechanical consequence of these structural abnormalities was an increase in yield load (+2.1 s.d., permuted $P = 8 \times 10^{-3}$) that reflected increased material elasticity (**Fig. 4**). Although the phenotype of *Gpc6*$^{-/-}$ mice is consistent with human omodysplasia 1, no information is available regarding adult manifestations of the condition. Thus, further studies in *Gpc6*$^{-/-}$ mice are required to characterize the cellular and molecular mechanisms underlying the role of GPC6 in the pathogenesis of osteoporosis.

Finally, we queried 87 separate GWASs using the web utility PhenoScanner, with full genome-wide summary statistics available for the conditionally independent genome-wide significant SNPs for eBMD (rs72635657, rs147720516) at the *GPC6* locus, for any associations with a P value of <0.05 (ref. 38). We identified one association, for rs72635657 with femoral neck BMD ($P = 0.015$). We also searched the NHGRI–EBI catalog[39] of published GWASs for *GPC6* (accessed 22 March 2017). SNPs in the region of *GPC6* had previously shown evidence of association with attention deficit hyperactivity disorder, FEV1 after bronchodilation, Alzheimer's disease, neuroticism and lower facial height, although the lead SNPs reported in these scans were not in appreciable LD with the lead conditionally independent SNPs in the present study (all $r^2 < 0.1$).

DISCUSSION

With this study, we have increased the number of genetic loci associated with BMD in humans almost threefold and doubled the amount of variance explained for this trait. Further, we have demonstrated that several BMD-associated variants also influence the risk of fracture. We have prioritized genes for future study and provided functional evidence that *GPC6* has a role in determining BMD and the pathophysiology of osteoporosis.

Our findings provide evidence that the genetic architecture underlying BMD is highly polygenic. The observed effect sizes follow a close relationship with MAF within the limits of the statistical power of the study. This suggests that further low-frequency and rare variants of moderate to large effect will be identified in future studies, which is likely to improve the overall understanding of the cellular and molecular mechanisms involved. Drug targets supported by evidence from human genetics are most likely to result in clinically useful therapies in general, and this has been demonstrated for musculoskeletal conditions[13,14]. Thus, our findings will be helpful for identifying pathways and proteins amenable to pharmacologic manipulation to decrease the burden of fracture in the population.

GPC6 encodes a glypican that may serve as a novel drug target for osteoporosis care, as it is a cell-surface protein involved in signaling whose loss of function leads to increased bone mineral content, likely due to increased cortical bone and resultant increased elasticity. GPC6 is a member of the glypican family (GPC1–6) of glycosylphosphatidylinositol-anchored, membrane-bound heparan sulfate proteoglycan core proteins that are involved in cellular growth control and differentiation. Mutations of *GPC3*, *GPC4* and *GPC6* result in developmental skeletal abnormalities, but limited or no information is available from affected adults (OMIM 312870, OMIM 258315). The heparan sulfate proteoglycans attached to the GPC6 core protein regulate skeletal signaling pathways involved in bone formation and mineralization, including those mediated by the FGF, VEGF, Hedgehog and BMP pathways[40]. In addition, the adult high-bone-mass phenotype and increased cortical bone thickness identified in *Gpc6*$^{-/-}$ mice in these studies is consistent with the recently identified direct role of GPC6 in the modulation of Wnt signaling[41,42], which is the key regulator of osteoblastic bone formation and is associated with BMD in humans. Overall, these findings suggest a number of possible new pharmacological targets that include not only the core protein GPC6, but also the heparan sulfate synthetic (EXT1–2) and modification enzymes (NDST1–4, GLCE, HS2ST and HS6ST1–3) that specifically regulate growth factor binding and activity. The availability of global and tissue-specific *Gpc6*$^{-/-}$ mice[35] now provides the opportunity to test these possibilities directly. However, we caution that although GPC6 and associated proteins seem to be promising targets for pharmacotherapy, other factors (the likelihood of unintended side effects, etc.) will need to be considered before these molecules can be confirmed as suitable candidates for pharmacological manipulation.

There are several limitations to our study. First, despite the high concordance between the loci identified from ultrasound-derived measurements of BMD and those from previous studies that used DXA-derived BMD, there were some notable differences. Our study did not replicate associations at 18 known BMD loci identified in previous studies. Also, our list of genome-wide significant variants included some that were strongly related to eBMD at the heel but were not found in previous studies that used DXA-derived BMD measures at other body sites in considerably smaller samples. For some of these loci, such as *TBX1*, this may simply be a consequence of the associated variants having been neither genotyped nor tagged well in previous studies. For other loci, it may reflect genetic influences that are specific to the heel (for example, genetic responses of the heel to ground reaction forces) that are not present at other body sites. Interestingly, we identified variants at six loci where the direction of effect was opposite between eBMD at the heel and DXA-derived BMD at other sites, although notably at *CPED1* the variants also showed association with risk of fracture in the direction consistent with the heel eBMD association. Although the reason for these differences is unclear, the implication is that ultrasound measurements of the heel capture aspects of bone structure beyond those obtained by central DXA, and this is consistent with previous observations that ultrasound measurements of the heel predict risk of osteoporotic fracture over and above hip BMD[43].

Second, our study does not provide a definitive biological mechanism through which variants at genome-wide significant loci causally affect eBMD. Our eQTL analyses were not consistent with the mediation of SNP effects through osteoblast expression at a majority of loci. This is probably because at least some of the identified eBMD-associated SNPs may act on cell types other than osteoblasts, such as osteocytes and osteoclasts. Further, the relatively small sample size of 95 individuals in the osteoblast eQTL experiment may have led to uncertain estimates. Also, the expression of genes in culture may reflect different biological processes than those *in vivo*. Although differences in gene expression are not the only mechanism through which the functional effects of an association can be mediated, we expect that large-scale genomic studies investigating the pattern of genetic association in osteoblasts, osteocytes and osteoclasts will reveal how these eBMD associations are mediated in the not-too-distant future.

Third, our study had a limited ability to detect very rare variants (i.e., MAF < 0.1%) or rare variants of small effect (MAF < 1% and effect size < 0.05 s.d.). Finally, our study investigated the genetic etiology of osteoporosis only in European individuals. It is likely that studies of populations of different ancestry will reveal novel loci that are important in the regulation of BMD, as has been the case for other conditions[44].

In summary, our findings shed light on the pathophysiological mechanisms that underlie changes in BMD and fracture risk in humans. The proteins identified and prioritized by these studies identify signaling pathways that represent new drug targets for the prevention and treatment of osteoporosis—a major health care priority.

URLs. International Mouse Phenotyping Consortium (IMPC), http://www.mousephenotype.org; Mouse Genome Informatics (MGI), http://www.informatics.jax.org; the Origins of Bone and Cartilage Disease Study (OBCD), http://www.boneandcartilage.com; UK Biobank (UKBB), http://www.ukbiobank.ac.uk/; Genetic Factors for Osteoporosis Consortium (GEFOS), http://www.gefos.org/; UK Biobank protocol for measurement of eBMD, https://biobank.ctsu.ox.ac.uk/crystal/docs/Ultrasoundbonedensitometry.pdf; UK Biobank document #155580 on genotyping and quality control, http://biobank.ctsu.ox.ac.uk/crystal/docs/genotyping_qc.pdf; Hg19 gene range list, https://www.cog-genomics.org/plink2/.

METHODS

Methods, including statements of data availability and any associated accession codes and references, are available in the online version of the paper.

Note: Any Supplementary Information and Source Data files are available in the online version of the paper.

ACKNOWLEDGMENTS

We thank P. Sham for helpful discussions and M. Schull for assistance with high-performance computing. We thank research nurses and assistants at the Departments of Surgical and Medical Sciences, Uppsala University, Uppsala, Sweden, for large-scale collection of bone samples and culture of primary osteoblasts. This part of the work was supported by Genome Quebec, Genome Canada and the Canadian Institutes of Health Research (CIHR). We thank T. Winkler for invaluable technical support for the EasyStrata Software used in this study.

This work was supported by the Medical Research Council (Programme Grant MC_UU_12013/4 to D.M.E.), the Wellcome Trust (Strategic Award grant number 101123; project grant 094134; to G.R.W., J.H.D.B. and P.I.C.), the Netherlands Organization for Health Research and Development ZonMw VIDI 016.136.367 (funding to F.R., C.M.-G. and K.T.), the mobility stimuli plan of the European Union Erasmus Mundus Action 2: ERAWEB (programme funding to K.T.), NIAMS, NIH (AR060981 and AR060234 to C.L.A.-B.), the National Health and Medical Research Council (Early Career Fellowship APP1104818 to N.M.W.), the Swedish Research Council (funding to E.G.), the Réseau de Médecine Génétique Appliquée (RMGA; J.A.M.), the Fonds de Recherche du Québec–Santé (FRQS; J.A.M. and J.B.R.), the Natural Sciences and Engineering Research Council of Canada (C.M.T.G.), the J. Gibson and the Ernest Heine Family Foundation (P.I.C.), Arthritis Research UK (ref. 20000; to C.L.G.), the Canadian Institutes of Health Research (J.B.R.), the Jewish General Hospital (J.B.R.), and the Australian Research Council (Future Fellowship FT130101709 to D.M.E.).

This research was conducted using the UK Biobank Resource (application number 12703). Access to the UK Biobank study data was funded by the University of Queensland (Early Career Researcher Grant 2014002959 to N.M.W.).

AUTHOR CONTRIBUTIONS

S.K., F.R., J.H.T., P.I.C., C.L.A.-B., J.H.D.B., G.R.W., J.B.R. and D.M.E. conceived and designed experiments. J.P.K., J.A.M., C.M.-G., V.F., N.M.W., S.E.Y., J.Z., K.T., E.G., K.M.G., C.X., C.M.T.G., C.L.A.-B., J.H.D.B. and G.R.W. performed statistical analysis. J.P.K., J.A.M., C.M.-G., V.F., N.M.W., S.E.Y., C.L.G., K.T., C.M.T.G., M.T.M., S.K., F.R., J.H.T., P.I.C., C.L.A.-B., J.H.D.B., G.R.W., J.B.R. and D.M.E. wrote the paper. S.E.Y., E.J.G., J.G.L., A.S.P., P.C.S., R.A., V.D.L., N.C.B., D.K.-E., A.-T.A., K.F.C., J.K.W., F.K., D.J.A., P.I.C., C.L.A.-B., J.H.D.B. and G.R.W. generated mouse models and/or functional experiments. N.C.H. and C.C. generated heel eBMD data. J.P.K., J.A.M. and C.M.-G. were the lead analysts. All authors revised and reviewed the paper.

COMPETING FINANCIAL INTERESTS

The authors declare no competing financial interests.

1. Cauley, J.A. *et al.* Long-term risk of incident vertebral fractures. *J. Am. Med. Assoc.* **298**, 2761–2767 (2007).
2. Liu, C.T. *et al.* Heritability of prevalent vertebral fracture and volumetric bone mineral density and geometry at the lumbar spine in three generations of the Framingham study. *J. Bone Miner. Res.* **27**, 954–958 (2012).
3. Estrada, K. *et al.* Genome-wide meta-analysis identifies 56 bone mineral density loci and reveals 14 loci associated with risk of fracture. *Nat. Genet.* **44**, 491–501 (2012).
4. Zheng, H.F. *et al.* Whole-genome sequencing identifies EN1 as a determinant of bone density and fracture. *Nature* **526**, 112–117 (2015).
5. Arden, N.K., Baker, J., Hogg, C., Baan, K. & Spector, T.D. The heritability of bone mineral density, ultrasound of the calcaneus and hip axis length: a study of postmenopausal twins. *J. Bone Miner. Res.* **11**, 530–534 (1996).
6. Howard, G.M., Nguyen, T.V., Harris, M., Kelly, P.J. & Eisman, J.A. Genetic and environmental contributions to the association between quantitative ultrasound and bone mineral density measurements: a twin study. *J. Bone Miner. Res.* **13**, 1318–1327 (1998).
7. Hunter, D.J. *et al.* Genetic variation in bone mineral density and calcaneal ultrasound: a study of the influence of menopause using female twins. *Osteoporos. Int.* **12**, 406–411 (2001).
8. Lee, M. *et al.* Unique and common genetic effects between bone mineral density and calcaneal quantitative ultrasound measures: the Fels Longitudinal Study. *Osteoporos. Int.* **17**, 865–871 (2006).

9. Bauer, D.C. *et al.* Broadband ultrasound attenuation predicts fractures strongly and independently of densitometry in older women. A prospective study. *Arch. Intern. Med.* **157**, 629–634 (1997).
10. Bauer, D.C. *et al.* Quantitative ultrasound predicts hip and non-spine fracture in men: the MrOS study. *Osteoporos. Int.* **18**, 771–777 (2007).
11. Gonnelli, S. *et al.* Quantitative ultrasound and dual-energy X-ray absorptiometry in the prediction of fragility fracture in men. *Osteoporos. Int.* **16**, 963–968 (2005).
12. Moayyeri, A. *et al.* Genetic determinants of heel bone properties: genome-wide association meta-analysis and replication in the GEFOS/GENOMOS consortium. *Hum. Mol. Genet.* **23**, 3054–3068 (2014).
13. Nelson, M.R. *et al.* The support of human genetic evidence for approved drug indications. *Nat. Genet.* **47**, 856–860 (2015).
14. Richards, J.B., Zheng, H.F. & Spector, T.D. Genetics of osteoporosis from genome-wide association studies: advances and challenges. *Nat. Rev. Genet.* **13**, 576–588 (2012).
15. Bulik-Sullivan, B.K. *et al.* LD score regression distinguishes confounding from polygenicity in genome-wide association studies. *Nat. Genet.* **47**, 291–295 (2015).
16. Duncan, E.L. *et al.* Genome-wide association study using extreme truncate selection identifies novel genes affecting bone mineral density and fracture risk. *PLoS Genet.* **7**, e1001372 (2011).
17. Koller, D.L. *et al.* Genome-wide association study of bone mineral density in premenopausal European-American women and replication in African-American women. *J. Clin. Endocrinol. Metab.* **95**, 1802–1809 (2010).
18. Richards, J.B. *et al.* Bone mineral density, osteoporosis, and osteoporotic fractures: a genome-wide association study. *Lancet* **371**, 1505–1512 (2008).
19. Rivadeneira, F. *et al.* Twenty bone-mineral-density loci identified by large-scale meta-analysis of genome-wide association studies. *Nat. Genet.* **41**, 1199–1206 (2009).
20. Styrkarsdottir, U. *et al.* Multiple genetic loci for bone mineral density and fractures. *N. Engl. J. Med.* **358**, 2355–2365 (2008).
21. Styrkarsdottir, U. *et al.* New sequence variants associated with bone mineral density. *Nat. Genet.* **41**, 15–17 (2009).
22. Xiong, D.H. *et al.* Genome-wide association and follow-up replication studies identified *ADAMTS18* and *TGFBR3* as bone mass candidate genes in different ethnic groups. *Am. J. Hum. Genet.* **84**, 388–398 (2009).
23. Wood, A.R. *et al.* Defining the role of common variation in the genomic and biological architecture of adult human height. *Nat. Genet.* **46**, 1173–1186 (2014).
24. Mackey, D.C. *et al.* High-trauma fractures and low bone mineral density in older women and men. *J. Am. Med. Assoc.* **298**, 2381–2388 (2007).
25. Sanders, K.M. *et al.* The exclusion of high trauma fractures may underestimate the prevalence of bone fragility fractures in the community: the Geelong Osteoporosis Study. *J. Bone Miner. Res.* **13**, 1337–1342 (1998).
26. Bulik-Sullivan, B. *et al.* An atlas of genetic correlations across human diseases and traits. *Nat. Genet.* **47**, 1236–1241 (2015).
27. Zheng, J. *et al.* LD Hub: a centralized database and web interface to perform LD score regression that maximizes the potential of summary level GWAS data for SNP heritability and genetic correlation analysis. *Bioinformatics* **33**, 272–279 (2017).
28. Ahmad, O.S. *et al.* A Mendelian randomization study of the effect of type-2 diabetes and glycemic traits on bone mineral density. *J. Bone Miner. Res.* **32**, 1072–1081 (2017).
29. Kemp, J.P., Sayers, A., Smith, G.D., Tobias, J.H. & Evans, D.M. Using Mendelian randomization to investigate a possible causal relationship between adiposity and increased bone mineral density at different skeletal sites in children. *Int. J. Epidemiol.* **45**, 1560–1572 (2016).
30. McLaren, W. *et al.* The Ensembl Variant Effect Predictor. *Genome Biol.* **17**, 122 (2016).
31. Kundaje, A. *et al.* Integrative analysis of 111 reference human epigenomes. *Nature* **518**, 317–330 (2015).
32. Thurman, R.E. *et al.* The accessible chromatin landscape of the human genome. *Nature* **489**, 75–82 (2012).
33. Grundberg, E. *et al.* Population genomics in a disease targeted primary cell model. *Genome Res.* **19**, 1942–1952 (2009).
34. Pers, T.H. *et al.* Biological interpretation of genome-wide association studies using predicted gene functions. *Nat. Commun.* **6**, 5890 (2015).
35. Skarnes, W.C. *et al.* A conditional knockout resource for the genome-wide study of mouse gene function. *Nature* **474**, 337–342 (2011).
36. Bassett, J.H. *et al.* Rapid-throughput skeletal phenotyping of 100 knockout mice identifies 9 new genes that determine bone strength. *PLoS Genet.* **8**, e1002858 (2012).
37. Campos-Xavier, A.B. *et al.* Mutations in the heparan-sulfate proteoglycan glypican 6 (GPC6) impair endochondral ossification and cause recessive omodysplasia. *Am. J. Hum. Genet.* **84**, 760–770 (2009).
38. Staley, J.R. *et al.* PhenoScanner: a database of human genotype-phenotype associations. *Bioinformatics* **32**, 3207–3209 (2016).
39. Welter, D. *et al.* The NHGRI GWAS Catalog, a curated resource of SNP-trait associations. *Nucleic Acids Res.* **42**, D1001–D1006 (2014).
40. Malinauskas, T. & Jones, E.Y. Extracellular modulators of Wnt signalling. *Curr. Opin. Struct. Biol.* **29**, 77–84 (2014).
41. Malinauskas, T., Aricescu, A.R., Lu, W., Siebold, C. & Jones, E.Y. Modular mechanism of Wnt signaling inhibition by Wnt inhibitory factor 1. *Nat. Struct. Mol. Biol.* **18**, 886–893 (2011).
42. Sakane, H., Yamamoto, H., Matsumoto, S., Sato, A. & Kikuchi, A. Localization of glypican-4 in different membrane microdomains is involved in the regulation of Wnt signaling. *J. Cell Sci.* **125**, 449–460 (2012).
43. Moayyeri, A. *et al.* Quantitative ultrasound of the heel and fracture risk assessment: an updated meta-analysis. *Osteoporos. Int.* **23**, 143–153 (2012).
44. Paternoster, L. *et al.* Multi-ancestry genome-wide association study of 21,000 cases and 95,000 controls identifies new risk loci for atopic dermatitis. *Nat. Genet.* **47**, 1449–1456 (2015).

ONLINE METHODS

Measurement of eBMD, fracture and weight in UK Biobank. In 2006–2010, the UK Biobank recruited 502,647 individuals aged 37–76 years (99.5% were aged 40–69 years) from across the country. All participants provided information regarding their health and lifestyle via touch screen questionnaires, consented to physical measurements, and agreed to have their health followed. They also provided blood, urine and saliva samples for future analysis. UK Biobank has ethical approval from the Northwest Multi-centre Research Ethics Committee, and informed consent was obtained from all participants. A Sahara Clinical Bone Sonometer (Hologic Corporation, Bedford, Massachusetts, USA) was used for quantitative ultrasound assessment of calcanei in UK Biobank participants. Details of the complete protocol are publicly available on the UK Biobank website ("URLs"). Participants were initially measured at baseline (N = 487,428) and had their left calcaneus (N = 317,815), right calcaneus (N = 4,102) or both calcanei (N = 165,511) measured. A subset of these subjects were followed up at two further time points (N = 20,104 and N = 7,988), during which both heels were measured. A detailed description of the ascertainment procedure is provided in **Supplementary Figure 2**. Prior to quality control, ultrasound data were available for 488,683 individuals at either baseline and/or follow-up assessment. eBMD (g/cm^2) was derived as a linear combination of speed of sound (SOS) and bone ultrasound attenuation (BUA) (eBMD = 0.002592 × (BUA + SOS) − 3.687). To reduce the impact of outlying measurements, quality control was applied to male and female subjects separately with the following exclusion thresholds: SOS, ≤1,450 or ≥1,700 m/s for males, ≤1,455 or ≥1,700 m/s for females; and BUA, ≤27 or ≥138 dB/MHz for males, ≤22 or ≥138 dB/MHz for females. Individuals exceeding the following thresholds for eBMD were excluded: males, ≤0.18 or ≥1.06 g/cm^2; females ≤0.12 or ≥1.025 g/cm^2. Bivariate scatter plots of eBMD, BUA and SOS were visually inspected, and any measurements that did not cluster with the others were removed; this left a total of 483,230 valid measures (476,618 left and 6,612 right calcaneus) for SOS, BUA and BMD (265,057 females and 218,173 males). Please see **Supplementary Figure 2** for a detailed description of the quality control pipeline and **Supplementary Table 1** for an overview of descriptive statistics of the cohort after quality control.

We defined 14,492 individuals (8,439 female and 6,053 male) as having a fracture, on the basis of affirmative answers to the question, "Have you fractured/broken any bones in the last 5 years?" at either baseline or first follow-up. Individuals were coded as missing if they responded "Do not know" or "Prefer not to answer" at both baseline and first follow-up; otherwise they were coded as controls (N = 130,563). Self-reported fractures have low false positive and false negative rates[45]. Individuals who stated that they had had a fracture were also asked whether the fracture resulted from a simple fall (i.e., from standing height). We created a second variable using this question, where 8,540 individuals (5,853 female and 2,687 male) had a fracture from a simple fall and 131,333 individuals did not report a fracture. Weight was measured with a Tanita BC418MA body composition analyzer.

Preparation, quality control and genetic analysis in UK Biobank samples. Genotype data from the interim May 2015 release of UK Biobank were available for a subset of 152,729 participants. Data were imputed centrally by UK Biobank with IMPUTE2 (ref. 46) to a 1000 Genomes (October 2014) and UK10K reference panel. In addition to the quality control metrics performed centrally by UK Biobank (UK Biobank document #155580; see "URLs"), we defined a subset of 'white European' ancestry samples by using a K-means (K = 4) clustering approach based on the first four genetically determined principal components. A maximum of 142,487 individuals (76,067 females and 66,420 males) with genotype and valid quantitative ultrasound measures were available for the present analyses. We tested genetic variants for association with eBMD, assuming an additive allelic effect, in a linear mixed non-infinitesimal model implemented in BOLT-LMM[47] to account for cryptic population structure and relatedness. Genotyping array, age and sex were included as covariates in all models. We also included weight as a covariate in a sensitivity analysis to investigate whether the power to detect association was increased or whether weight mediated the relationship between genotype and eBMD (i.e., some variants may be primarily associated with weight, and their effect on eBMD may be mediated through a causal effect of weight on eBMD[29]). Only SNPs down to an MAF of 0.1% and with an info-score threshold of >0.4 were analyzed. We additionally analyzed the association between eBMD and directly genotyped SNPs on the X chromosome, adjusting for genotyping array, age, sex and the first four ancestry principal components, using Plink v1.09 beta 3.38 (7 June 2016) software[48] and a nested sample of unrelated subjects (N = 135,729). Because the analyses for the X chromosome data were based on observed genotypes, our quality control was slightly different. We excluded SNPs with evidence of deviation from Hardy–Weinberg equilibrium (1×10^{-6}), MAF < 0.1% and overall missing rate > 5%, which yielded 15,552 X chromosome SNPs for analysis. Heterogeneity between sexes in effect size coefficients was tested with EasyStrata[49]. Manhattan and Miami plots of our genome-wide association scans were generated by EasyStrata version 15.3. Regional association plots were generated with LocusZoom (v1.3)[50], using LD information estimated from our reference UK Biobank sample, together with the December 2016 release of the NHGRI–EBI catalog of published GWASs. SNPs that were associated with eBMD at genome-wide significance levels were additionally tested for association with fracture using BOLT-LMM, including age, sex, BMI and the time of reporting the fracture as fixed effects[47].

Estimation of genome-wide significance threshold. Traditional estimates of the genome-wide significance threshold for common variants (MAF > 5%) in European populations (i.e., $\alpha = 5 \times 10^{-8}$) are based on a Bonferroni correction of $\alpha = 0.05/10^6$, as there are an estimated 1 million statistically independent SNPs above this MAF threshold. However, in the case of UK Biobank, we assessed SNPs down to an MAF of 0.1% in 142,487 individuals and applied an info-score threshold of >0.4, which resulted in 17.17 million SNPs. Thus, we defined a new and more conservative threshold to declare genome-wide significance, accounting for the number of independent statistical tests performed in our data. To do this, we applied the method we used previously in the UK10K sequencing consortium[4], which assesses the correlation between nearby test statistics empirically. Analysis of permuted data derived from a small proportion of all tested variants allows assessment of the correlation patterns. Thus we were able to estimate, in subsets of the genome of varying size, the relationship between the Bonferroni significance threshold and the empirical significance threshold that corrects for correlations, and thereby extrapolate to the whole genome. Specifically, when assessing all 740,018 variants that met our filtering criteria across chromosome 9 (**Supplementary Fig. 9**), we saw a good linear fit between family-wise error rate ($\alpha = 0.05$), divided by the number of tests and the empirical significance thresholds. Our estimated genome-wide significance threshold then, accounting for all SNPs with MAF ≥ 0.1% and info-score > 0.4, was $\alpha = 6.6 \times 10^{-9}$.

Approximate conditional association analysis. To detect multiple independent association signals at each of the genome-wide significant eBMD loci, we carried out approximate conditional and joint genome-wide association analysis using the software package GCTA[51]. SNPs with high collinearity (multiple regression R^2 > 0.9) were ignored, and those situated more than 20 Mb away were assumed to be in complete linkage equilibrium. A reference sample of 15,000 unrelated (pairwise relatedness < 0.025) individuals of white British origin randomly selected from UK Biobank was used to model patterns of LD between variants. The reference genotyping data set consisted of the same 17 million variants assessed in our GWAS, but with an additional quality control step to exclude SNPs that deviated from Hardy–Weinberg equilibrium (1×10^{-6}). Conditionally independent variants that reached GWAS significance were annotated to the physically closest gene with bedtools[52] v2.26.0 and the Hg19 Gene range list available online (see "URLs").

Estimation of variance explained by significant variants and SNP heritability. We estimated the proportion of phenotypic variance tagged by all SNPs on the genotyping array (i.e., the SNP heritability) with BOLT-REML[53]. To calculate the variance explained by all genome-wide significant SNPs, we first used the method of Bigdeli *et al.*[54] to shrink the effect sizes of SNPs likely to suffer from 'winner's curse'. Briefly, the method works by shrinking the effect sizes of SNPs that just reach significance while having a negligible effect on SNPs that are more robustly significant (and consequently more accurately and precisely estimated). After calculating the corrected effect sizes, we removed the combined effect of the SNPs on the individual's eBMD and recalculated the total expected variance in BOLT-LMM. The difference between this estimate

and the total expected variance calculated on the original data without the SNP correction was an estimate of the variance explained by all SNPs.

Linkage disequilibrium score regression. To estimate the amount of genomic inflation in the data due to residual population stratification, cryptic relatedness and other latent sources of bias, we used LD score regression[15]. LD scores were calculated for all high-quality SNPs (i.e., INFO score > 0.9 and MAF > 0.1%) from a data set consisting of 15,000 unrelated individuals from the UK Biobank. To estimate the genetic correlation between eBMD and other complex traits and diseases, including those related to osteoporosis, we used a relatively new method based on LD score regression as implemented in the online web utility LDHub[26,27]. This method uses the cross-products of summary test statistics from two GWASs and regresses them against a measure of how much variation each SNP tags (its LD score). Variants with high LD scores are more likely to contain more true signals and thus provide a greater chance of overlap with genuine signals between GWASs. The LD score regression method uses summary statistics from the GWAS meta-analysis of eBMD and the other traits of interest, calculates the cross-product of test statistics at each SNP, and then regresses the cross-product on the LD score. The slope of the regression is a function of the genetic covariance between traits:

$$E(z_{1j}z_{2j}) = \frac{\sqrt{N_1N_2}\rho_g}{M} l_j + \frac{\rho N_S}{\sqrt{N_1N_2}}$$

where N_i is the sample size for study i, ρ_g is the genetic covariance, M is the number of SNPs in the reference panel with MAFs between 5% and 50%, l_j is the LD score for SNP j, N_s quantifies the number of individuals that overlap both studies, and ρ is the phenotypic correlation among the N_s overlapping samples. Thus, if there is sample overlap (or cryptic relatedness between samples), it will affect only the intercept from the regression (i.e., the term $\rho N_s / \sqrt{N_1N_2}$) and not the slope, and hence estimates of the genetic covariance will not be biased by sample overlap. Likewise, population stratification will affect the intercept but will have a minimal effect on the slope (i.e., intuitively, as population stratification does not correlate with LD between nearby markers).

Gene prioritization and pathway analysis. To establish functional connections, we conducted three different analyses implemented in the DEPICT v1 tool[34]. First, to prioritize genes with relevant biological roles in the eBMD-associated loci, we tested functional similarities among genes from different associated regions where genes with high functional similarity across regions obtained lower prioritization *P* values. Second, we analyzed expression enrichment across particular tissues or cell types by testing whether genes in the associated eBMD loci had high expression in any of the 209 MeSH annotations, using data from 37,427 expression arrays. Third, we performed a gene set enrichment analysis to test whether the genes in the associated eBMD loci were enriched in reconstituted gene sets. The 10,968 gene sets tested were generated from diverse databases, including Gene Ontology, KEGG, REACTOME, the InWeb database (high-confidence protein–protein interaction), and the Mouse Genetics Initiative (phenotype–genotype relationships). In all three analyses we used the FDR to adjust for multiple testing; significance was defined at FDR = 5%.

The DEPICT analyses were based on independent lead SNPs ($r^2 < 0.1$; European populations, 1000 Genomes reference panel) with *P* values below the genome-wide significance threshold ($P < 6.64 \times 10^{-9}$). Because many of the gene sets tested came from different repositories, they overlapped; hence significantly enriched gene sets were further grouped into 'meta gene sets' through similarity clustering, as previously described[34]. The visualization of these meta gene-sets was performed in Cytoscape[55], filtering at FDR < 1%.

We also compared the DEPICT gene set enrichment results to analyses with the MAGENTA software[56]. Briefly, MAGENTA maps each gene in the genome to a single index SNP with the lowest *P* value within a 110-kb upstream and 40-kb downstream window (excluding genes in the HLA region owing to complex patterns of LD). This *P* value is then corrected for confounding factors (SNP density, gene size, etc.) in a linear regression model, and each gene is ranked by its adjusted gene score. The observed number of gene scores in a given pathway, with a ranked score above a specified threshold (i.e., 95th and 75th percentiles of all gene scores), is then calculated. This observed statistic is then compared to 1,000,000 randomly permuted pathways of identical size. This generates an empirical gene set enrichment analysis *P* value for each gene set. A gene set was declared significant when an individual pathway reached FDR < 0.05 in either analysis. We tested 3,217 prespecified gene sets from the Gene Ontology, Ingenuity, KEGG, Protein Analysis through Evolutionary Relationships (PANTHER), BioCarta and Reactome databases.

Prioritizing candidate genes and possible causal variants at each eBMD locus. We combined a number of approaches to identify possible causal SNPs at each eBMD signal (defined here as all SNPs within 500 kb of a conditionally independent lead SNP that attained genome-wide significance). First, we used the Variant Effect Predictor (VEP)[30] to annotate all SNPs within a locus (defined as ±500 kb from a conditionally independent lead SNP) for deleterious coding variation annotation if they were significantly associated with eBMD ($P < 6.6 \times 10^{-9}$). Deleterious SNPs were classified as such if they had one of the following sequence ontology terms: frameshift_variant, inframe_deletion, inframe_insertion, initator_codon_variant, missense_variant, splice_acceptor_variant, splice_donor_variant, stop_gained, or stop_lost.

Next, using FINEMAP[57], we identified 305 autosomal lead SNPs and further defined sets of plausible causal SNPs within each locus. For each locus, FINEMAP implements a shotgun stochastic search algorithm to test multiple causal configurations of SNPs, calculating within a Bayesian framework the posterior probabilities of each configuration to identify the number of likely causal SNPs. We note that this approach assumes that the true causal variants have been included in the analysis and have been well imputed. We also emphasize that approaches such as this that are based solely on association test statistics and LD are unlikely to be definitive with respect to the identification of causal variants/genes. Thus, we regard these fine-mapping analyses as one of several approaches that can be used to implicate specific variants/genes in osteoporosis etiology. When the same variant/gene is implicated by multiple independent approaches (for example, mouse knockout, human knockout, gene expression and eQTL studies), there is greater confidence of the identity of the gene/variant(s) underlying the statistical association.

For a given number of plausible causal SNPs, FINEMAP will calculate for each SNP the Bayes factor, which quantifies the evidence that the particular SNP is causal. We retained only SNPs with Bayes factors greater than 100, or $\log_{10}$ Bayes factors greater than 2, as our plausible causal SNPs for each locus.

We then annotated each set of plausible causal SNPs for overlap with DHSs, using a master list derived from 115 cell types[4]. DHSs are focal sites of open chromatin comprising the collective transcription factor binding sites in a given cell type. We further annotated each SNP inhabiting a DHS with Contextual Analysis of Transcription Factor Occupancy (CATO) scores. CATO, previously described by Maurano *et al.*[4], scores the likelihood that a variant will cause allelic imbalance of a DHS by modeling both local sequence context and direct effects on the transcription factor recognition sequences for 44 transcription factor motif families. CATO scores range between 0 and 1, and we considered SNPs with CATO scores greater than 0.1 as having very strong functional evidence (corresponding to a 51% positive predictive rate in the initial training set[4]).

Genetically modified animals used for functional validation. The IMPC ("URLs")[58] and the International Knockout Mouse Consortium (IKMC) are generating null alleles for all protein-coding genes in mice on a C57BL/6 genetic background[59]. These mice are phenotyped through a broad-based phenotyping screen[60]. This approach can be used for functional investigation of candidate genes identified by a GWAS of human disease or traits, and studies have already ascribed novel functions for poorly annotated or previously unpublished genes. The Origins of Bone and Cartilage Disease (OBCD) study ("URLs") is undertaking a validated multiparameter skeletal phenotype screen[36] of mutant mouse lines generated by the Wellcome Trust Sanger Institute as part of the IKMC and IMPC effort.

OBCD methods. Samples from 16-week-old female wild-type and knockout mice were stored in 70% ethanol, anonymized and randomly assigned to batches for rapid-throughput analysis in an unselected fashion. The relative bone mineral content (BMC) and length of the femur and caudal vertebrae

doi:10.1038/ng.3949

were determined at 10-μm pixel resolution by digital X-ray microradiography (Faxitron MX20). Micro-CT (Scanco uCT50, 70 kV, 200 μA, 0.5-mm aluminum filter) was used to determine cortical bone parameters (thickness, BMD, medullary diameter) at 10-μm voxel resolution in a 1.5-mm region centered on the mid-shaft region 56% of the way along the length of the femur distal to the femoral head, and trabecular parameters (bone volume, trabecular number, thickness, spacing) at 5-μm voxel resolution in a 1-mm region beginning 100 μm proximal to the distal growth plate. Biomechanical variables of bone strength and toughness (yield load, maximum load, fracture load, the percentage of energy dissipated before fracture) were derived from destructive three-point bend testing of the femur and compression testing of caudal vertebrae 6 and 7 (Instron 5543 load frame, 100-N load cell)[36]. Overall, 19 skeletal parameters were reported for each individual mouse studied and compared to reference data obtained from >250 16-week-old wild-type C57BL/6 female mice. Coefficients of variation for each skeletal parameter were as follows: femur BMC (2.0%) and length (2.1%); vertebra BMC (2.1%) and length (2.3%); trabecular bone volume/tissue volume (18.5%), trabecular number (7.3%), trabecular thickness (7.9%) and trabecular spacing (8.3%); cortical bone thickness (4.3%), internal diameter (6.0%) and BMD (4.0%); femur yield load (13.2%), maximum load (10.0%), fracture load (29.0%), stiffness (13.7%) and energy dissipated before fracture (26.7%); and vertebra yield load (13.0%), maximum load (10.3%) and stiffness (13.3%).

In **Supplementary Table 15**, we highlight knockout mice with phenotypes greater than 2 s.d. away from the mean of wild-type mice. We generated *P* values for the reported *Gpc6*$^{-/-}$ mouse phenotypes through permutation. To do so we first identified the least extreme phenotype for the *Gpc6*$^{-/-}$ mice tested. We then permuted the knockout labels 100,000 times to observe the number of times we observed two knockout animals with both phenotypes as extreme as the least extreme *Gpc6*$^{-/-}$ mouse phenotype. The *P* value was then calculated as the number of extreme permutations divided by 100,000. All mouse studies were undertaken by the Wellcome Trust Sanger Institute Mouse Genetics Project as part of the IKMC and licensed by the UK Home Office in accordance with the Animals (Scientific Procedures) Act 1986 and the recommendations of the Weatherall report.

Gene expression in primary human and mouse osteoblasts. To study human osteoblasts, we undertook *cis*-eQTL analyses of plausible causal regulatory SNPs in 95 primary human osteoblasts as previously described by Grundberg *et al.*[33], performed with an updated imputation panel, the combined UK10K and 1000 Genomes phase 1 v3 reference panel[61]. We used an α level of 0.05 to identify possible gene targets of plausible causal SNPs.

We investigated the possibility that heel eBMD associations and *cis*-eQTL effects in osteoblasts may represent different signals (as opposed to a causal effect of osteoblast expression on eBMD) by performing two sample summary Mendelian randomization analyses on osteoblast eQTL and heel eBMD GWAS results[62,63]. A HEIDI (heterogeneity in dependent instruments) test was used to identify situations in which the lead *cis*-eQTL was likely to be in LD with two distinct causal variants (one affecting gene expression, and the other affecting eBMD variation), as opposed to expression of the relevant gene mediating the relationship between the SNP and eBMD. Intuitively the test works by comparing estimates of the putative causal effect of gene expression on eBMD obtained by Mendelian randomization analysis of each variant while taking into account dependencies between the SNPs. Under a causal model, different SNPs should produce the same causal estimate (subject to sampling error), whereas under a model of linkage (i.e., two separate signals in the region, one affecting gene expression in osteoblasts and the other affecting eBMD), the estimates from the Mendelian randomization analysis may significantly differ. In the context of our study, a significant HEIDI test suggested that expression of the relevant gene in osteoblasts does not mediate the SNP–eBMD association. We therefore performed HEIDI tests for all the probes listed in **Supplementary Table 10** that were implicated in our gene expression analyses. To prevent weak SNP instruments from potentially affecting our results, we included only SNPs that exhibited strong evidence of association (i.e., *F* statistic > 10) in the eQTL analysis[63].

Gene expression profiles of candidate genes were examined in primary mouse osteoblasts undergoing differentiation. These data have been described in detail previously[64] and are publicly available from the Gene Expression Omnibus (GSE54461). To study mouse osteoblasts, we obtained pre-osteoblast-like cells from calvaria collected from neonatal C57BL/6J mice carrying a transgene expressing cyan florescent protein (CFP) under the control of the Col 3.6-Kb promoter. The cells were placed into culture for 4 d in growth media, and cells that did not express CFP at the end of that culture period were removed by FACS. The remaining pre-osteoblast cells were re-plated and exposed to an osteoblast-differentiation cocktail, and RNA was collected every 2 d from day 2 to 18 d post-differentiation. We used RNA-seq to evaluate the transcriptome at each time point with an Illumina HiSeq 2000. Three technical replicates per samples were sequenced. The alignments for abundance estimation of transcripts were created with Bowtie version 0.12.9, using the NCBIM37 reference genome. We calculated the expression level per gene with RSEM version 1.2.0 with parameters of --fragment-length-mean 280 and --fragment-length-sd 50, and the expression level for each sample was normalized relative to the per-sample upper quartile.

Gene expression in mouse osteocytes. We determined osteocyte expression by analyzing whole-transcriptome sequences derived from four different mouse bones: the tibia, femur, humerus and calvaria (marrow removed; $n = 8$ per bone). A threshold of expression was determined on the basis of the distribution of normalized gene expression for each sample, using a modified statistical approach from Hart *et al.*[64]. 'Expressed' genes were above this threshold for eight of eight replicates in any bone type. We determined the specificity of these genes' expression in the skeleton by comparing transcriptome-sequencing data from bone samples with osteocytes isolated to data from bones with the marrow left intact ($n = 5$ per group) (S.E.Y., J.H.D.B., G.R.W., and P.I.C., manuscript in preparation).

Gene expression in mouse osteoclasts. Expression of genes in mouse osteoclasts was determined from publically available data obtained via RNA-seq of bone-marrow-derived osteoclasts obtained from 6–8-week-old C57BL/6 mice (GEO accession GSM1873361).

Data availability. The human genotype and phenotype data on which the results of this study are based are available upon application from UK Biobank ("URLs"). GWAS summary statistics from this study are available via the GEFOS website ("URLs"). No new data sets or related accession codes were generated as part of this study. Mouse phenotype data are available online from the IMPC ("URLs") and OBCD ("URLs").

A **Life Sciences Reporting Summary** for this paper is available.

45. Ismail, A.A. *et al.* Validity of self-report of fractures: results from a prospective study in men and women across Europe. *Osteoporos. Int.* **11**, 248–254 (2000).
46. Howie, B., Marchini, J. & Stephens, M. Genotype imputation with thousands of genomes. *G3 (Bethesda)* **1**, 457–470 (2011).
47. Loh, P.R. *et al.* Efficient Bayesian mixed-model analysis increases association power in large cohorts. *Nat. Genet.* **47**, 284–290 (2015).
48. Chang, C.C. *et al.* Second-generation PLINK: rising to the challenge of larger and richer datasets. *Gigascience* **4**, 7 (2015).
49. Winkler, T.W. *et al.* EasyStrata: evaluation and visualization of stratified genome-wide association meta-analysis data. *Bioinformatics* **31**, 259–261 (2015).
50. Pruim, R.J. *et al.* LocusZoom: regional visualization of genome-wide association scan results. *Bioinformatics* **26**, 2336–2337 (2010).
51. Yang, J. *et al.* Conditional and joint multiple-SNP analysis of GWAS summary statistics identifies additional variants influencing complex traits. *Nat. Genet.* **44**, 369–375 (2012).
52. Quinlan, A.R. & Hall, I.M. BEDTools: a flexible suite of utilities for comparing genomic features. *Bioinformatics* **26**, 841–842 (2010).
53. Loh, P.R. *et al.* Contrasting genetic architectures of schizophrenia and other complex diseases using fast variance-components analysis. *Nat. Genet.* **47**, 1385–1392 (2015).
54. Bigdeli, T.B. *et al.* A simple yet accurate correction for winner's curse can predict signals discovered in much larger genome scans. *Bioinformatics* **32**, 2598–2603 (2016).
55. Saito, R. *et al.* A travel guide to Cytoscape plugins. *Nat. Methods* **9**, 1069–1076 (2012).
56. Segrè, A.V., Groop, L., Mootha, V.K., Daly, M.J. & Altshuler, D. Common inherited variation in mitochondrial genes is not enriched for associations with type 2 diabetes or related glycemic traits. *PLoS Genet.* **6**, e1001058 (2010).

57. Benner, C. *et al.* FINEMAP: efficient variable selection using summary data from genome-wide association studies. *Bioinformatics* **32**, 1493–1501 (2016).
58. Koscielny, G. *et al.* The International Mouse Phenotyping Consortium Web Portal, a unified point of access for knockout mice and related phenotyping data. *Nucleic Acids Res.* **42**, D802–D809 (2014).
59. International Mouse Knockout Consortium. *A mouse for all reasons. Cell* **128**, 9–13 (2007).
60. de Angelis, M.H. *et al.* Analysis of mammalian gene function through broad-based phenotypic screens across a consortium of mouse clinics. *Nat. Genet.* **47**, 969–978 (2015).
61. Huang, J. *et al.* Improved imputation of low-frequency and rare variants using the UK10K haplotype reference panel. *Nat. Commun.* **6**, 8111 (2015).
62. Evans, D.M. & Davey Smith, G. Mendelian randomization: new applications in the coming age of hypothesis-free causality. *Annu. Rev. Genomics Hum. Genet.* **16**, 327–350 (2015).
63. Zhu, Z. *et al.* Integration of summary data from GWAS and eQTL studies predicts complex trait gene targets. *Nat. Genet.* **48**, 481–487 (2016).
64. Hart, T., Komori, H.K., LaMere, S., Podshivalova, K. & Salomon, D.R. Finding the active genes in deep RNA-seq gene expression studies. *BMC Genomics* **14**, 778 (2013).

doi:10.1038/ng.3949

nature research

Corresponding author(s): DAVID M EVANS
J BRENT RICHARDS

☐ Initial submission ☐ Revised version ☒ Final submission

Life Sciences Reporting Summary

Nature Research wishes to improve the reproducibility of the work that we publish. This form is intended for publication with all accepted life science papers and provides structure for consistency and transparency in reporting. Every life science submission will use this form; some list items might not apply to an individual manuscript, but all fields must be completed for clarity.

For further information on the points included in this form, see Reporting Life Sciences Research. For further information on Nature Research policies, including our data availability policy, see Authors & Referees and the Editorial Policy Checklist.

Experimental design

1. Sample size

   Describe how sample size was determined.

   Skeletal phenotyping of knockout mice.
   The reference ranges for each skeletal parameter were derived from >250 female 16 week old C57BL/6 wild-type mice. Using these data together with coefficients of variation for each test, power calculations indicate an 80% power to detect outlier phenotype of greater or equal to 2SD with a sample size of n=2

2. Data exclusions

   Describe any data exclusions.

   If skeletal samples were damaged or incomplete on receipt they were excluded from the analysis.

3. Replication

   Describe whether the experimental findings were reliably reproduced.

   No replication of knockout mouse lines.

4. Randomization

   Describe how samples/organisms/participants were allocated into experimental groups.

   Not applicable

5. Blinding

   Describe whether the investigators were blinded to group allocation during data collection and/or analysis.

   All skeletal samples from knockout mice generated by the Wellcome Trust Sanger Institute were bar coded. Samples were sent to Imperial College in anonymized batches and all skeletal phenotyping and analysis was performed blind to genotype.

Note: all studies involving animals and/or human research participants must disclose whether blinding and randomization were used.

Nature Genetics: doi:10.1038/ng.3949

6. Statistical parameters

For all figures and tables that use statistical methods, confirm that the following items are present in relevant figure legends (or in the Methods section if additional space is needed).

n/a	Confirmed
☐	☒ The exact sample size (*n*) for each experimental group/condition, given as a discrete number and unit of measurement (animals, litters, cultures, etc.)
☒	☐ A description of how samples were collected, noting whether measurements were taken from distinct samples or whether the same sample was measured repeatedly
☒	☐ A statement indicating how many times each experiment was replicated
☐	☒ The statistical test(s) used and whether they are one- or two-sided (note: only common tests should be described solely by name; more complex techniques should be described in the Methods section)
☒	☐ A description of any assumptions or corrections, such as an adjustment for multiple comparisons
☐	☒ The test results (e.g. *P* values) given as exact values whenever possible and with confidence intervals noted
☐	☒ A clear description of statistics including central tendency (e.g. median, mean) and variation (e.g. standard deviation, interquartile range)
☒	☐ Clearly defined error bars

See the web collection on statistics for biologists for further resources and guidance.

Software

Policy information about availability of computer code

7. Software

Describe the software used to analyze the data in this study.	NA

For manuscripts utilizing custom algorithms or software that are central to the paper but not yet described in the published literature, software must be made available to editors and reviewers upon request. We strongly encourage code deposition in a community repository (e.g. GitHub). *Nature Methods* guidance for providing algorithms and software for publication provides further information on this topic.

Materials and reagents

Policy information about availability of materials

8. Materials availability

Indicate whether there are restrictions on availability of unique materials or if these materials are only available for distribution by a for-profit company.	All knockout lines and primary phenotype data are available on line at the IMPC http://www.mousephenotype.org/ and OBCD http://www.boneandcartilage.com/

9. Antibodies

Describe the antibodies used and how they were validated for use in the system under study (i.e. assay and species).	NA

10. Eukaryotic cell lines

a. State the source of each eukaryotic cell line used.	NA
b. Describe the method of cell line authentication used.	NA
c. Report whether the cell lines were tested for mycoplasma contamination.	NA
d. If any of the cell lines used are listed in the database of commonly misidentified cell lines maintained by ICLAC, provide a scientific rationale for their use.	NA

Nature Genetics: doi:10.1038/ng.3949

Animals and human research participants

Policy information about studies involving animals; when reporting animal research, follow the ARRIVE guidelines

11. Description of research animals

Provide details on animals and/or animal-derived materials used in the study.

Knockout mice were generated at the Wellcome Trust Sanger Institute for the International Mouse Phenotyping Consortium. Skeletal samples from female 16 week old C57BL/6 wild type and mutant mice in an identical genetic background were analysed.

Policy information about studies involving human research participants

12. Description of human research participants

Describe the covariate-relevant population characteristics of the human research participants.

NA

Nature Genetics: doi:10.1038/ng.3949